

Non-thermal emission from old supernova remnants

Jun Fang^{1*}, Li Zhang^{1,2}

¹*Department of Physics, Yunnan University, Kunming, PRC*

²*National Astronomical Observatories/Yunnan Observatory, Chinese Academy of Sciences, P.O. Box 110, Kunming, PRC*

2 November 2018

ABSTRACT

We study the non-thermal emission from old shell-type supernova remnants (SNRs) on the frame of a time-dependent model. In this model, the time-dependent non-thermal spectra of both primary electrons and protons as well as secondary electron/positron (e^\pm) pairs can be calculated numerically by taking into account the evolution of the secondary e^\pm pairs produced from proton-proton (p-p) interactions due to the accelerated protons collide with the ambient matter in an SNR. The multi-wavelength photon spectrum for a given SNR can be produced through leptonic processes such as electron/positron synchrotron radiation, bremsstrahlung and inverse Compton scattering as well as hadronic interaction. Our results indicate that the non-thermal emission of the secondary e^\pm pairs is becoming more and more prominent when the SNR ages in the radiative phase because the source of the primary electrons has been cut off and the electron synchrotron energy loss is significant for a radiative SNR, whereas the secondary e^\pm pairs can be produced continuously for a long time in the phase due to the large energy loss time for the p-p interaction. We apply the model to two old SNRs, G8.7–0.1 and G23.3–0.3, and the predicted results can explain the observed multi-wavelength photon spectra for the two sources.

Key words: radiation mechanisms: non-thermal – supernova remnants – ISM: individual: G8.7–0.1, G23.3–0.3 – gamma-rays: theory

1 INTRODUCTION

In recent years, various observational evidences indicate that particles in SNRs can be accelerated up to relativistic energies. For example, X-ray observations show that electrons can be accelerated to about 10 TeV in the shell of an SNR (Koyama et al. 1995; Reynolds 1996; Bamba et al. 2003, 2005a, 2005b). TeV γ -ray observations indicate that both electrons and protons can be accelerated to several tens TeV in young shell-type SNRs such as RX J1713.7–3946 (Enomoto et al. 2002; Aharonian et al. 2006a) and RX J0852.0–4622 (Katagiri et al. 2005; Aharonian et al. 2005). More recently, a survey of the inner part of the Galactic Plane in VHE γ -ray band has been performed with *HESS* Cherenkov telescope system. Aharonian et al. (2006b) presented detailed spectral and morphological information of some new sources discovered in the *HESS* survey along with some discussions on possible counterparts in other wavelength bands. Some sources discovered in the survey can be associated with old SNRs. For example, HESS J1804–216 has a flux of nearly 25% of the flux of the Crab Nebula with a photon index of about 2.72. The source can be associated with either the shell-type SNR G8.7–2.1 or

the young Vela-like pulsar PSR J1803–2137 (Aharonian et al. 2006b). Furthermore, Fatuzzo, Melia, & Crocker (2006) found that the SNR G8.7–2.1 can plausibly account for all known radiative characteristics of HESS J1804–216. Another case is HESS J1834–087, which is an extended TeV source discovered in the *HESS* survey of the inner Galaxy in VHE γ -ray band. The source, spatially coincident with the SNR G23.3–0.3, has a γ -ray flux of 8% of the flux of the Crab Nebula above 200 GeV, and the γ -ray spectrum can be expressed by a power law with a photon index of 2.45 ± 0.16 (Aharonian et al. 2006b). The new *XMM-Newton* observation reveals diffuse X-ray emission within the *HESS* source and suggests an association between the diffuse X-rays and the VHE γ -rays, moreover, G23.3–0.3 is estimated to be an old SNR with a distance of 4 ± 0.2 kpc and an age of $\sim 10^5$ yr (Tian et al. 2007).

Theoretically, it is believed that the non-thermal photon spectrum for a given SNR is produced through electron/positron synchrotron radiation, bremsstrahlung and inverse Compton scattering as well as π^0 decay from the p-p interactions. The question is, however, whether the origin of the non-thermal photons for young SNRs is different from that for old ones. Sturmer et al. (1997) presented a temporal evolution model to calculate the non-thermal particle and photon spectra from shell-type SNRs, and Zhang &

* email: fangjun1653@126.com

Fang (2007) modified the model to investigate the possible hadronic contributions to TeV γ -ray emission from young SNRs. For the young SNRs, the secondary particles produced via the p-p interaction have a negligible contribution to the non-thermal photon spectrum (e.g. Zhang & Fang 2007). On the other hand, Yamazaki et al. (2006) studied the emission from old SNRs and found that proton acceleration could be efficient enough to emit TeV γ -rays both at the shock of the SNR and at the giant molecular cloud. They presented that the energy flux ratio $R_{\text{TeV}/X}$ can be more than 10^2 for some SNRs, and such sources may be the origins of the recently discovered unidentified TeV sources. For the old SNRs, the energies of the primary electrons accelerated by the shock wave are limited by the synchrotron cooling, then the roll-off energy of the synchrotron emission of the primary electrons is much smaller than that for the young SNRs (Sturmer et al. 1997; Yamazaki et al. 2006; Zhang & Fang 2007). However, the secondary e^\pm pairs can be produced from the p-p collisions in an SNR for a long time due to the large energy loss time for the p-p interaction. Therefore, the contributions of secondary electrons and positrons to the non-thermal emission can become prominent for the old SNRs.

Motivated by above discussions, we study the non-thermal photon spectra from old SNRs based on the time-dependent model in which the contribution of the secondary e^\pm pairs is included (see §2.2). It should be noted that our model is different from that given by Yamazaki et al. (2006), the latter assumes a steady particle distribution. This paper is organized as follows. The temporally evolving model of the non-thermal particle and photon spectra are discussed in Section 2, including the SNR evolution, shock acceleration, and various photon production mechanisms involved in the model. The results from the applications of the model to two old SNRs, G8.7–0.1 and G23.3–0.3, are shown in Section 3. The main conclusions and some discussions are given in Section 4.

2 TEMPORAL MODEL FOR MULTI-WAVELENGTH NON-THERMAL EMISSION FROM SNRS

Sturmer et al. (1997) presented a temporally-evolving model for the non-thermal particle and photon spectra at different stages in the lifetime of a shell-type SNR. Zhang & Fang (2007) modified the model to explain the multi-wavelength observations of the young SNRs and shown that the TeV γ -rays from the two young shell-type SNRs RX J1713.7–3946 and RX J0852.0–4622 have hadronic origin. In this paper, we include the evolution of secondary e^\pm pairs to model the multi-wavelength non-thermal emission from old SNRs since the secondary e^\pm pairs can have significant contributions to the non-thermal emission from old SNRs.

2.1 SNR Evolution and Shock Acceleration

In the analytical model of the shock dynamics of an SNR expanding into a uniform ambient medium with density n_0 , the SNR evolves through three stages: the free expansion stage, the Sedov stage, and the radiative stage (Sturmer et al. 1997;

Yamazaki et al. 2006). Assuming the initial explosion energy of the SNR is $E = 10^{51} E_{51}$ ergs, and the initial velocity of the shock is v_0 , the free expansion stage ends when $t = t_{\text{Sed}} = (3E/2\pi m_H n_0 v_0^5)^{1/3} \approx 2.1 \times 10^2 (E_{51}/n_0)^{1/3} v_0^{-5/3}$ yr, and the Sedov stage ends at $t = t_{\text{rad}} \approx 4.0 \times 10^4 E_{51}^{4/17} n_0^{-9/17}$ yr (Blondin et al. 1998), where $n_0 = \mu n_{\text{ISM}}$, n_{ISM} is the hydrogen density in the local interstellar medium, $\mu = 1.4$ is the mean atomic weight of the interstellar medium assuming 1 helium atom for every 10 hydrogen atoms, and m_H is the mass of hydrogen. The shock velocity $v_s(t)$ can be expressed as (e.g. Yamazaki et al. 2006)

$$v_s(t) = \begin{cases} v_0 & t < t_{\text{Sed}} \\ v_0 \left(\frac{t}{t_{\text{Sed}}}\right)^{-3/5} & t_{\text{Sed}} \leq t < t_{\text{rad}} \\ v_0 \left(\frac{t_{\text{rad}}}{t_{\text{Sed}}}\right)^{-3/5} \left(\frac{t}{t_{\text{rad}}}\right)^{-2/3} & t_{\text{rad}} \leq t. \end{cases} \quad (1)$$

The evolution of the shock radius is estimated by $R_s(t) = \int v_s(t) dt$ and we assume $v_0 = 10^9 \text{ cm s}^{-1}$ in this paper. It should be noted that the accumulated energy in non-thermal protons for an SNR is usually smaller than 10% of the initial explosion energy (see details in §2.1), and the energy diminishes very slowly in the radiative phase when the thermal energy in the SNR experiences significant loss. At late times, the relativistic protons begin to contribute significantly to the post-shock pressure when most thermal energy of the SNR is drained and then the expansion law should be revised correspondingly. However, the expansion law will be influenced significantly by the accelerated protons at very late times and the non-thermal emission from old SNRs does not depend heavily on the expansion law. Therefore, we still assume the expansion law expressed by Eq. (1) is always valid in this paper.

It is generally believed that the non-thermal charged particles are produced through diffusive shock acceleration (Blandford & Eichler 1987; Ellison, Jones & Reynolds 1990). Neglecting the nonlinear effects and assuming a compression ratio near 4, the particle spectrum from the diffusive acceleration process is a power law with spectral index $\alpha \sim 2$. For the particles accelerated in the shock of an SNR, the power law particle spectra do not extend to infinite energy and must be truncated by three mechanisms, namely, the finite age of the SNR, energy-loss processes, and free escape from the shock region (Sturmer et al. 1997). The maximum kinetic energy of electrons and protons, $E_{e, \text{max}}$ and $E_{p, \text{max}}$, can be calculated by using Eqs. (3), (4), (5) in Sturmer et al. (1997), and we neglect the exact formulae here. Zhang & Fang (2007) studied the non-thermal emission from three young SNRs, and concluded that the model in the paper can explain the multi-wavelength observations for the three young SNRs with the maximum wavelength of MHD turbulence $\lambda_{\text{max}} = 2 \times 10^{17} \text{ cm}$ and other appropriate parameters. λ_{max} is also set to $2 \times 10^{17} \text{ cm}$ in this paper.

It should be pointed out that a time-dependent kinetic equation could be solved in order to obtain the energy spectrum of the accelerated particles (Berezhko et al. 1996; Sturmer et al. 1997). Here, following Sturmer et al. (1997), we approximate the volume-averaged emissivity, $Q(E, t) = dN/dV dt dE$, of the shock accelerated electrons and protons by

$$Q_e^{\text{pri}}(E, t) = Q_e^0 G(t) [E(E + 2m_e c^2)]^{-(\alpha+1)/2}$$

$$\times (E + m_e c^2) \exp\left(-\frac{E}{E_{e, \max}(t)}\right), \quad (2)$$

and

$$Q_p^{\text{pri}}(E, t) = Q_p^0 G(t) [E(E + 2m_p c^2)]^{-(\alpha+1)/2} \times (E + m_p c^2) \exp\left(-\frac{E}{E_{p, \max}(t)}\right), \quad (3)$$

respectively, where E is the particle kinetic energy, and m_e and m_p are electron mass and proton mass, the index $\alpha \sim 2.0$, and we use $\alpha = 2.0$ in this paper. The function $G(t)$ is given by (Sturmer et al. 1997)

$$G(t) = \begin{cases} [R_{\text{SNR}}(t_{\text{Sed}})/R_{\text{SNR}}(t)] & t \leq t_{\text{rad}} \\ 0 & t > t_{\text{rad}}. \end{cases} \quad (4)$$

Factors Q_e^0 and Q_p^0 are used to normalize the particle spectra so that the total amount of the kinetic energy contained in the injected electrons and protons is $E_{\text{par}} = \eta M_{\text{ej}} v_0^2 / 2$, where $\eta \sim 0.1$ represents the efficiency that the kinetic energy of the ejecta with initial mass M_{ej} and initial velocity v_0 is converted into the kinetic energy of both the electrons and the protons,

$$E_{\text{par}} = \int_0^{t_{\text{rad}}} dt V_{\text{SNR}}(t) \left(\int_0^{E_{e, \max}} dE E Q_e^{\text{pri}}(E, t) + \int_0^{E_{p, \max}} dE E Q_p^{\text{pri}}(E, t) \right), \quad (5)$$

and $V_{\text{SNR}}(t) = 4\pi R_{\text{SNR}}^3(t)/3$ is the SNR volume. In Eq. (5), we need to introduce the parameter $K_{\text{ep}} = Q_e^0/Q_p^0$ in order to determine Q_e^0 and Q_p^0 . Obviously, these two quantities depend on η and K_{ep} . The ratio of electrons to protons, K_{ep} , is a key parameter when modeling the multi-wavelength non-thermal emission from an SNR. The measured ratio from the cosmic ray observations at the Earth is about 0.013 at 10 GeV (Gassier 1990). However, the measured value can not represent the ratio for a given SNR due to the cosmic ray transport effect in the Galaxy. Sturmer et al. (1997) obtained $K_{\text{ep}} \sim 0.6$ by assuming that the kinetic energy of the injected electrons is the same as that of the injected protons. Yamazaki et al. (2006) studied the TeV emission from the old SNRs in the steady state, they used the observed ratio of TeV γ -ray (1–10 TeV) to X-ray (2–10 keV) energy flux, $R_{\text{TeV/X}}$, for some SNRs to test the values of K_{ep} , and found that the predicted $R_{\text{TeV/X}}$ for young SNRs is similar to the observed one when $K_{\text{ep}} = 1 \times 10^{-3}$, and that the predicted values of $R_{\text{TeV/X}}$ for the old SNRs are not changed even if K_{ep} varies more than one order of magnitude because the primary electrons do not contribute to TeV and X-ray emission in their model. Moreover, Berezhko, Ksenofontov & Völk (2006) investigated the properties of Kepler's SNR using the nonlinear kinetic theory of cosmic ray acceleration in the SNR. They treated K_{ep} as a parameter quantitatively determined by comparison with the synchrotron observations and obtained that $K_{\text{ep}} \sim 10^{-4}$ for the SNR. In fact, the value of K_{ep} for a given source is usually uncertain now, and it can be limited by comparison of the resulting spectrum with the multi-wavelength observations for an SNR (Zhang & Fang 2007). In this paper, η is set to 0.1 and K_{ep} is treated as a parameter limited by comparison of the calculated results with the observations for a given SNR.

2.2 Temporal Evolution of Particle Energy Distributions

Following Sturmer et al. (1997), assuming that an SNR interior is homogeneous, with a constant density $n_{\text{SNR}} = 4n_{\text{ISM}}$ and a magnetic field strength $B_{\text{SNR}} = 4B_{\text{ISM}}$, $n_e(E_e, t)$ and $n_p(E_p, t)$ are used to represent the differential densities of the accelerated electrons and protons, respectively. We can use Q_e and Q_p to calculate the direction- and volume-averaged electron intensity $J_e(E_e, t) = (c\beta/4\pi)n_e(E_e, t)$ and proton intensity $J_p(E_p, t) = (c\beta/4\pi)n_p(E_p, t)$ at each moment during the SNR lifetime. Fokker-Planck equations for both electrons and protons in energy space are used to find solutions, which are given by (Sturmer et al. 1997)

$$\begin{aligned} \frac{\partial n_e(E_e, t)}{\partial t} &= -\frac{\partial}{\partial E_e} \left[\dot{E}_e^{\text{tot}} n_e(E_e, t) \right] \\ &+ \frac{1}{2} \frac{\partial^2}{\partial E_e^2} [D(E_e, t) n_e(E_e, t)] \\ &+ Q_e(E_e, t) - \frac{n_e(E_e, t)}{\tau}, \end{aligned} \quad (6)$$

and

$$\begin{aligned} \frac{\partial n_p(E_p, t)}{\partial t} &= -\frac{\partial}{\partial E_p} \left[\dot{E}_p^{\text{tot}} n_p(E_p, t) \right] \\ &+ \frac{1}{2} \frac{\partial^2}{\partial E_p^2} [D(E_p, t) n_p(E_p, t)] \\ &+ Q_p(E_p, t) - \frac{n_p(E_p, t)}{\tau}, \end{aligned} \quad (7)$$

respectively, where the terms on the right-hand sides in Eqs. (6) and (7) represent systematic energy losses, diffusion in energy space, the particle source function and catastrophic energy loss. Following Sturmer et al. (1997), we solve the above equations using a Crank-Nicholson finite difference scheme. In Eqs. (6) and (7), \dot{E}_e^{tot} , $D(E_e, t)$, \dot{E}_p^{tot} and $D(E_p, t)$ can be calculated with the formulae in §2.2 in Zhang & Fang (2007), the exact expressions are neglected in this paper.

The secondary electrons and positrons can be produced when the accelerated protons collide with the ambient matter via the p-p interaction. Those secondary particles evolve with the SNR, and can contribute to the multi-waveband non-thermal emission from the SNR as the primary electrons. So the source term for electron can be represented as

$$Q_e(E, t) = Q_e^{\text{pri}} + Q_{e^+}^{\text{sec}}(E, t) + Q_{e^-}^{\text{sec}}(E, t), \quad (8)$$

where

$$Q_{e^+}^{\text{sec}}(E, t) = 4\pi\mu_{\text{pp}}n_{\text{SNR}} \int dE_p J_p(E_p, t) \frac{d\sigma(E_{e^+}, E_p)}{dE_{e^+}}, \quad (9)$$

$$Q_{e^-}^{\text{sec}}(E, t) = 4\pi\mu_{\text{pp}}n_{\text{SNR}} \int dE_p J_p(E_p, t) \frac{d\sigma(E_{e^-}, E_p)}{dE_{e^-}}, \quad (10)$$

$\mu_{\text{pp}} = 1.45$ is a enhancement factor for collisions involving heavy nuclei in an SNR (Dermer 1996; Sturmer et al. 1997), $d\sigma(E_{e^-}, E_p)/dE_{e^-}$ and $d\sigma(E_{e^+}, E_p)/dE_{e^+}$ are the differential cross section for electrons and positrons produced via p-p interaction, respectively. Since the accelerated protons colliding with the ambient medium (i.e. p-p interaction) can produce pions (π^\pm and π^0), in which a proton loses $\sim 1/3$ of its energy per pion-producing collision, there exists the catastrophic loss for the protons. Sturmer et al. (1997)

treated this process as an escape from the system, and the timescale for this catastrophic loss is

$$\tau_{\text{pion}}(E_p) = [c\beta_p n_{\text{SNR}} \sigma_{\text{pp}}]^{-1}, \quad (11)$$

where σ_{pp} is the inelastic cross section for p-p interaction, which is (Kelner et al. 2006)

$$\sigma_{\text{pp}}(E_p) = (34.3 + 1.88L + 0.25L^2) \left[1 - \left(\frac{E_{\text{th}}}{E_p} \right)^4 \right] \text{ mb}, \quad (12)$$

where $L = \ln(E_p/1\text{TeV})$, $E_{\text{th}} = m_p + 2m_\pi + m_\pi^2/2m_p$ is the threshold energy of production of π -mesons.

2.3 Photon Production

We can solve the Eqs. (6) and (7) to get the volume- and direction-averaged intensities for electrons and protons at a given time, and then the multi-waveband non-thermal photon spectra can be calculated. The non-thermal radiation processes of the accelerated particles involved in an SNR are synchrotron radiation, bremsstrahlung, inverse Compton scattering for leptons including electrons and positrons, and the p-p interaction for protons.

Accelerated electrons can emit photons via synchrotron radiation as interacting with the ambient magnetic field in an SNR. The emissivity for synchrotron radiation is given by

$$Q_{\text{syn}}(E_\gamma, t) = \left(\frac{2\sqrt{3}e^3 B_{\text{SNR}}}{\hbar E_\gamma m_e c^3} \right) \int_0^{\pi/2} d\theta \sin^2 \theta \times \int_{E_{e,\text{min}}}^{E_{e,\text{max}}} dE_e J_e(E_e, t) F\left(\frac{E_\gamma}{E_c}\right), \quad (13)$$

where θ is the electron pitch angle, $E_c = 4.2 \times 10^6 \hbar B_{\text{SNR}} \gamma_e^2 \sin \theta$, and

$$F(y) = y \int_y^\infty dz K_{5/3}(z) \quad (14)$$

with $y = E_\gamma/E_c$, where $K_{5/3}$ is a modified Bessel function of order 5/3.

For the electron-electron and electron-nucleon bremsstrahlung radiation, the emissivity is (Sturmer et al. 1997)

$$Q_{\text{brem}}(E_\gamma, t) = 4\pi n_{\text{SNR}} \Delta_{\text{He}}^{e,n} \times \int_{E_{e,\text{min}}}^{E_{e,\text{max}}} dE_e J_e(E_e, t) \left(\frac{d\sigma}{dE_\gamma} \right)_{e-e,p} \quad (15)$$

where Δ_{He}^e and Δ_{He}^n are correction factors for the presence of helium ($\Delta_{\text{He}}^e = 1.2$ and $\Delta_{\text{He}}^n = 1.4$), $d\sigma_{e-e}/dE_\gamma$ and $d\sigma_{e-p}/dE_\gamma$ represent the differential electron-electron and electron-nucleon bremsstrahlung cross sections. Here, we use the approximate formulae given in Baring et al. (1999).

We use the full Klein-Nishina cross section for the relativistic electrons to tackle the inverse Compton process, the emissivity can be expressed as

$$Q_{\text{comp},j}(E_\gamma, t) = 4\pi \int_0^\infty d\epsilon n_j(\epsilon, r) \int_{E_{e,\text{thresh}}}^{E_{e,\text{max}}} dE_e \times J_e(E_e, t) F(\epsilon, E_\gamma, E_e), \quad (16)$$

where, ϵ is the target photon energy, n_j is the number density of soft photon component j with energy density U_j and temperature T_j and is given by

$$n_j(\epsilon) = \frac{15U_j}{(\pi k T_j)^4} \frac{\epsilon^2}{\exp(\epsilon/kT_j) - 1}, \quad (17)$$

$E_{e,\text{thresh}} = [E_\gamma + (E_\gamma^2 + E_\gamma(m_e c^2)^2/\epsilon)^{1/2}]/2$ is the lowest energy that electrons can scatter a target photon with energy ϵ to energy E_γ . Function $F(\epsilon, E_\gamma, E_e)$ is given by

$$F(\epsilon, E_\gamma, E_e) = \frac{3\sigma_T}{4(E_e/mc^2)^2} \frac{1}{\epsilon} \times \left[2q \ln q + (1+2q)(1-q) + \frac{(\Gamma q)^2(1-q)}{2(1+\Gamma q)} \right], \quad (18)$$

with $\Gamma = 4\epsilon(E_e/mc^2)/mc^2$, $q = E_1/\Gamma(1-E_1)$ with $E_1 = E_\gamma/E_e$ and $1/4(E_e/mc^2) < q < 1$.

Kamae et al. (2006) presented a series of accurate, convenient parameterized formulae to calculate the spectra of stable secondary particles (γ , e^\pm , ν_e , $\bar{\nu}_e$, ν_μ , $\bar{\nu}_\mu$) produced in the p-p interactions, which greatly facilitate calculations involving the p-p interaction in astronomical environments. The formulae were derived from the up-to-date p-p interaction model given by Kamae et al. (2005), which incorporates the logarithmically rising inelastic cross section, the diffraction dissociation process, and the Feynman scaling violation. The functional formula reproducing the secondary particle spectra include the non-diffractive, diffractive, and resonance-excitation components. For the nondiffractive process, the differential inclusive cross section to produce a secondary particle is given as

$$\frac{d\sigma_{\text{ND}}(E_{\text{sec}})}{d \ln(E_{\text{sec}})} = F_{\text{ND}}(x) F_{\text{ND,kl}}(x), \quad (19)$$

where E_{sec} is the energy of the secondary particle, $x = E_{\text{sec}}/\text{GeV}$, $F_{\text{ND}}(x)$ is the formula representing the non-diffractive cross section, and $F_{\text{ND,kl}}(x)$ is the formula to approximately enforce the energy-momentum conservation limits:

$$F_{\text{ND}}(x) = a_0 \exp(-a_1(x - a_3 + a_2(x - a_3)^2)^2) + a_4 \exp(-a_5(x - a_8 + a_6(x - a_8)^2) + a_7(x - a_8)^3)^2), \quad (20)$$

$$F_{\text{ND,kl}} = \frac{1}{\exp[W_{\text{ND,l}}(L_{\text{min}} - x)] + 1} \times \frac{1}{\exp[W_{\text{ND,h}}(x - L_{\text{max}})] + 1}, \quad (21)$$

where L_{min} and L_{max} are the lower and upper kinematic limits imposed and $W_{\text{ND,l}}$ and $W_{\text{ND,h}}$ are the widths of the kinematic cutoffs, $L_{\text{min}} = -2.6$ for all secondary particles, and the other parameters are given in Table 1 (Kamae et al. 2006).

The differential inclusive cross section to produce a secondary particle for the diffractive process can be represented as

$$\frac{d\sigma_{\text{diff}}(E_{\text{sec}})}{d \ln(E_{\text{sec}})} = F_{\text{diff}}(x) F_{\text{kl}}(x), \quad (22)$$

where $F_{\text{diff}}(x)$ represents the diffractive cross section, and $F_{\text{kl}}(x)$ is a function to enforce the energy-momentum conservation:

$$F_{\text{diff}}(x) = b_0 \exp(-b_1((x - b_2)/(1 + b_3(x - b_2)))^2) + b_4 \exp(-b_5((x - b_6)/(1 + b_7(x - b_6)))^2), \quad (23)$$

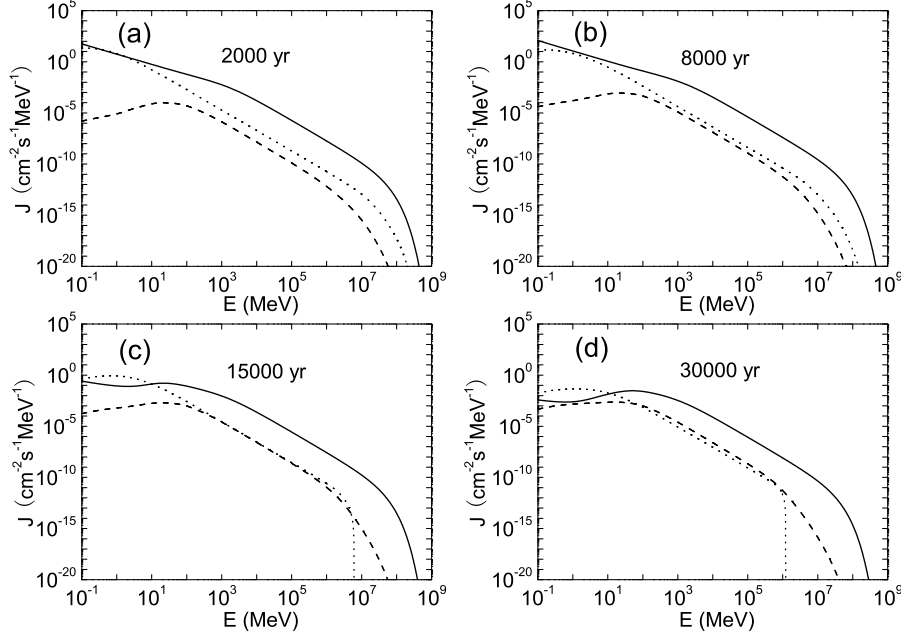


Figure 1. The isotropic intensities of the primary electrons (dotted line), the primary protons (solid line), and the secondary e^\pm pairs (dashed line) at (a) 2000, (b) 8000, (c) 15000, and (d) 30000 yr, respectively, for $M_{\text{ej}} = 1.5M_\odot$, $n_{\text{ISM}} = 10 \text{ cm}^{-3}$, $B_{\text{ISM}} = 5 \mu\text{G}$, $K_{\text{ep}} = 0.001$.

Table 1. Kinematic limit parameters for the nondiffractive process (Kamae et al. 2006).

	L_{max}	$W_{\text{ND},l}$	$W_{\text{ND},h}$
γ	$0.96 \log_{10}(T_p)$	15	44
e^-	$0.96 \log_{10}(T_p)$	20	45
e^+	$0.94 \log_{10}(T_p)$	15	47
ν_e	$0.98 \log_{10}(T_p)$	15	42
$\bar{\nu}_e$	$0.98 \log_{10}(T_p)$	15	40
ν_μ	$0.94 \log_{10}(T_p)$	20	45
$\bar{\nu}_\mu$	$0.98 \log_{10}(T_p)$	15	40

$$F_{\text{kl}}(x) = \frac{1}{\exp(W_{\text{diff}}(x - L_{\text{max}})) + 1}, \quad (24)$$

here $W_{\text{diff}} = 75$, $L_{\text{max}} = \log_{10}(T_p/\text{GeV})$.

For the resonance-excitation processes, the function is

$$\frac{d\sigma_{\text{res}}(E_{\text{sec}})}{d \ln(E_{\text{sec}})} = F_{\text{res}}(x) F_{\text{kl}}(x), \quad (25)$$

$F_{\text{res}}(x)$ represents the cross section, and $F_{\text{kl}}(x)$, which is same as that for the diffraction process, enforces the energy-momentum conservation:

$$F_{\text{res}}(x) = c_0 \exp(-c_1((x - c_2)/(1 + c_3(x - c_2) + c_4(x - c_2)^2))^2). \quad (26)$$

A renormalization factor, $r(T_p)$, must be multiplied to the final spectrum to ensure that the parameterized model reproduces the experimental π^0 multiplicity after the readjustment in the resonance-excitation region of T_p . The ex-

act expressions for $r(T_p)$ and other parameters involved in the formulae are shown in Kamae et al. (2006). Finally, the differential cross section for the secondary particles can be expressed as

$$\begin{aligned} \frac{d\sigma(E_{\text{sec}}, E_p)}{dE_{\text{sec}}} &= \frac{d\sigma_{\text{ND}}(E_{\text{sec}}, E_p)}{dE_{\text{sec}}} + \frac{d\sigma_{\text{diff}}(E_{\text{sec}}, E_p)}{dE_{\text{sec}}} \\ &+ \frac{d\sigma_{\Delta(1232)}(E_{\text{sec}}, E_p)}{dE_{\text{sec}}} \\ &+ \frac{d\sigma_{\text{res}(1600)}(E_{\text{sec}}, E_p)}{dE_{\text{sec}}}. \end{aligned} \quad (27)$$

The resulting particle intensities calculated with the model are shown in Fig. 1. The parameters we choose are $M_{\text{ej}} = 1.5M_\odot$, $n_{\text{ISM}} = 10 \text{ cm}^{-3}$, $B_{\text{ISM}} = 5 \mu\text{G}$, $K_{\text{ep}} = 0.001$, for ages of 2000, 8000, 15000, 30000 yr. For these parameters, the primary particle sources turn off at $t = t_{\text{rad}} = 1.01 \times 10^4$ yr. The turnover at the low energy region for both electrons and protons is due to Coulomb loss, and the high-energy turnover for electrons is due to synchrotron loss. More importantly, the primary electrons dominate the secondary e^\pm pairs for a young age, however, the secondary e^\pm pairs become more and more important and eventually surpass the primary electrons as the age of the SNR increases, the reason is that the sources of the primary particles are cut off in the radiative phase of the SNR and the primary electrons experience strong synchrotron energy loss, however, the energy loss for the protons is negligible due to the small cross section for the p-p interaction, and then the secondary particles can be produced continuously for a long time.

We show the resulting multi-wavelength non-thermal

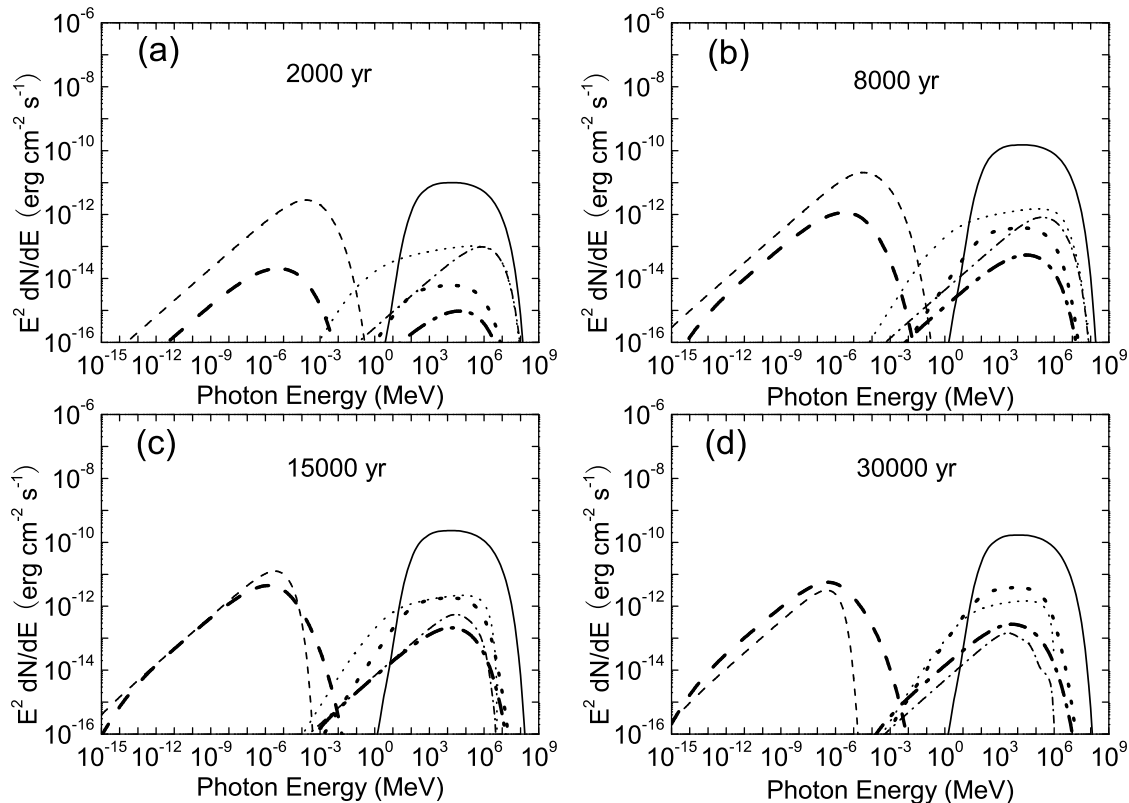


Figure 2. The resulting calculated multi-wavelength spectra at (a) 2000, (b) 8000, (c) 15000, and (d) 30000 yr, respectively. The distance is set to 2 kpc and the other parameters are same as those in Fig. 1. The emission due to synchrotron (dashed line), bremsstrahlung (dotted line), Compton scattering (dash-dotted line) of the primary electrons (thin) and the secondary e^\pm pairs (thick), and the p-p interaction (solid line) are shown in each panel.

spectra in Fig. 2. The distance to the SNR is chosen to be 2 kpc, and other parameters are same as those in Fig. 1. It is obvious that the emission from radio to X-ray band for the SNR comes from the synchrotron radiation of leptons, and the high-energy photons can from bremsstrahlung and inverse Compton scattering of leptons, and meson decay due to the hadronic interactions. More importantly, (1) the roll-off energy of the synchrotron radiation of the primary electrons decreases quickly when the SNR ages in the radiative phase, however, the synchrotron emission of the secondary e^\pm pairs become more and more important and eventually surpass the synchrotron radiation from the primary electrons when the SNR ages due to the secondary e^\pm pairs can be produced for a long time via the p-p interaction; (2) most VHE γ -rays from the SNR are of hadronic origin with those parameters, and the hadronic emission from an SNR is similar during a long time when the SNR is in the radiative phase because the energy loss rate for the contained protons is small. Of course, the photons with energy smaller than 10 MeV from some old SNRs mainly come from the radiation of the secondary e^\pm pairs.

3 APPLICATION TO OLD SNRS

3.1 SNR G8.7–0.1

Aharonian et al. (2006b) reported a survey of the inner part of the Galactic Plane in very high energy γ -rays observed with *HESS* Cherenkov telescope system, and fourteen previously unknown sources were detected at a significance level greater than 4σ after accounting for all trials involved in the search. A source detected in the survey is *HESS* J1804–216, which is the brightest one of the new sources, with a steep photon index of 2.72 ± 0.12 and a flux of nearly 25% of the flux from the Crab Nebula above 200 GeV. The source can be associated with the south-western part of the shell of the SNR G8.7–0.1 of radius 26 arc minutes with flux 80 Jy at 1 GHz (Green 2006), or the young Vela-like pulsar PSR J1803–2137 with a spin-down age of 16000 yr. Fatuzzo et al. (2006) presented a simple model for the TeV emission from *HESS* J1804–216, they found that the SNR G8.7–0.1 can plausibly account for all the known radiative characteristics of *HESS* J1804–216, and therefore the SNR G8.7–0.1 was probably the source of the TeV photons originating from the direction of *HESS* J1804–216.

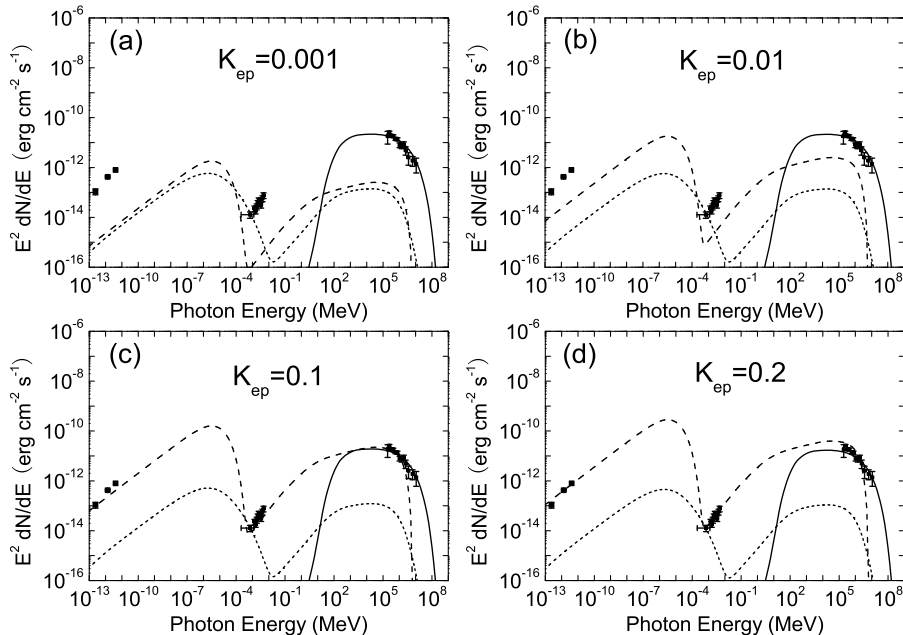


Figure 3. Comparisons of the model results with the multi-band observations for the SNR G8.7–0.1. The radiation from the primary electrons (dashed line), the primary protons (solid line), and the secondary e^\pm pairs (dotted line) with data points from Odegard (1986), Kassim & Weiler (1990), Green (2006) (radio), Cui & Konopelko (2006) (X-ray), Aharonian et al. (2006b) (*HESS*) are indicated in each panel. The parameters are a distance of 6 kpc, an age of 15000 yr, $M_{\text{ej}} = 1.5 M_\odot$, $n_{\text{ISM}} = 8 \text{ cm}^{-3}$, $B_{\text{ISM}} = 6 \mu\text{G}$, (a) $K_{\text{ep}} = 0.001$, (b) $K_{\text{ep}} = 0.01$, (c) $K_{\text{ep}} = 0.1$, (d) $K_{\text{ep}} = 0.2$.

By associating G8.7–0.1 with coincident HII regions, Kassim & Weiler (1990) estimated a distance to the SNR of 6 ± 1 kpc, with angular size of ~ 50 arcmin, a physical size of ~ 80 pc, and an age of 15000 yr. Cui & Konopelko (2006) reported the high-resolution X-ray observations taken with the Chandra X-Ray Observatory of the field that contains the TeV γ -ray source HESS J1804–216, and a total of 11 discrete sources were detected. Among those sources, only one, CXOU J180351.4–213707, is the most probable X-ray counterpart of HESS J1804–216, is significantly extended with photon index $1.2^{+0.5}_{-0.4}$.

We now assume that the sources CXOU J180351.4–213707 and HESS J1804–216 associate with the SNR G8.7–0.1. To make the resulting spectrum consistent with the observations by Chandra with a low energy flux and a photon index about 1.2, the SNR must be in the radiative phase when the roll-off energy of the synchrotron radiation of the primary electrons decreases quickly and the X-rays detected by Chandra X-Ray Observatory are most probably from the bremsstrahlung radiation or inverse Compton scattering of leptons, then n_{ISM} should be greater than $\sim 5 \text{ cm}^{-3}$ for an age of 15000 yr.

We now describe the detailed process in modeling the multi-waveband spectrum for the SNR. First of all, we investigate the influence of K_{ep} on the final spectra with parameters a distance of 6 kpc, an age of 15000 yr, $M_{\text{ej}} = 1.5 M_\odot$, $B_{\text{ISM}} = 6 \mu\text{G}$, and $n_{\text{ISM}} = 8 \text{ cm}^{-3}$ for the SNR G8.7–0.1. The calculated results are shown in Fig. 3. The spectrum

in the X-ray band depends heavily on K_{ep} , and the value of K_{ep} must be around 0.1 in order to match the observed data in X-ray band for the SNR.

Fig. 4 shows the resulting spectra from the SNR for different n_{ISM} and ages. For an age of 15000 yr, the roll-off energy of the synchrotron emission is still high for $n_{\text{ISM}} = 6 \text{ cm}^{-3}$, which conflicts with the Chandra observation, and the level of the TeV emission is greater than the observed one by HESS both for $n_{\text{ISM}} = 6 \text{ cm}^{-3}$ and for $n_{\text{ISM}} = 8 \text{ cm}^{-3}$ (see panel (a) and panel (b) in Fig. 4). The model results can fit the multi-band observations well with a larger age of 18000 yr, moreover, the calculated spectrum in the band 0.1–1 TeV for $n_{\text{ISM}} = 6 \text{ cm}^{-3}$ fit the TeV observations better than that for $n_{\text{ISM}} = 8 \text{ cm}^{-3}$ (see panel (c) and panel (d) in Fig. 4). Furthermore, the contributions to the final spectrum of different radiation components with the same parameters as those in panel (c) of Fig. 4 are shown in Fig. 5. Obviously from Fig. 5, for the SNR, (1) the emission from the primary electrons dominates that from the secondary e^\pm pairs in the entire energy band except in the narrow soft X-ray band around 0.5 keV; (2) the detected radio emission is mainly from the synchrotron radiation of the primary electrons whereas the X-rays observed with Chandra are primarily produced via the bremsstrahlung of these electrons; (3) the TeV photons with energies < 1 TeV are primarily from both the bremsstrahlung of the primary electrons and the p-p interaction of the primary protons, however, those with

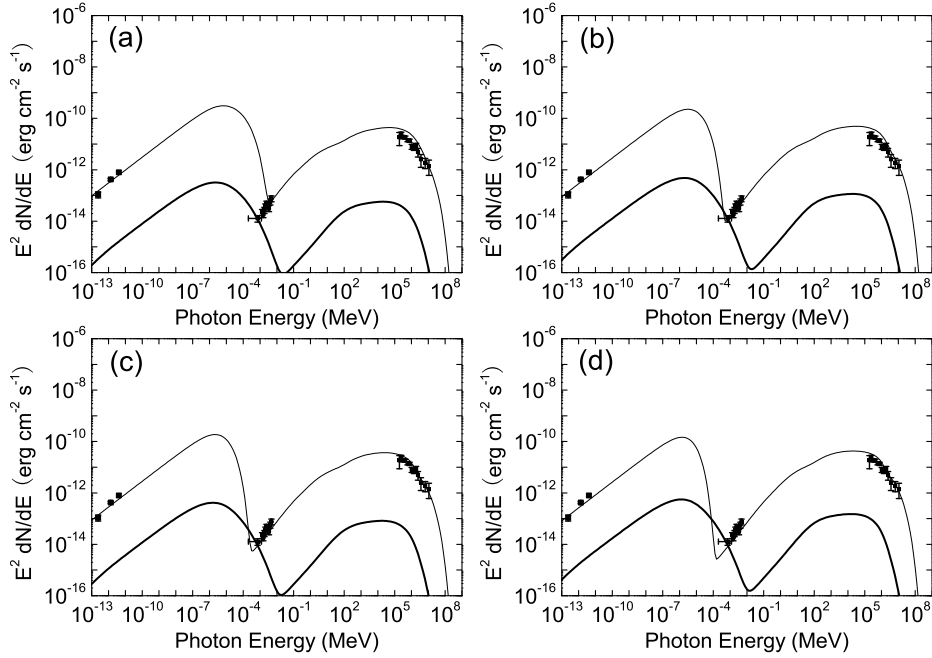


Figure 4. Comparisons of the model spectra with the observations for the SNR G8.7–0.1 with $K_{\text{ep}} = 0.15$, (a) $n_{\text{ISM}} = 6 \text{ cm}^{-3}$, an age of 15000 yr; (b) $n_{\text{ISM}} = 8 \text{ cm}^{-3}$, an age of 15000 yr; (c) $n_{\text{ISM}} = 6 \text{ cm}^{-3}$, an age of 18000 yr; (d) $n_{\text{ISM}} = 8 \text{ cm}^{-3}$, an age of 18000 yr. The whole emission from the primary particles and the secondary e^{\pm} pairs are indicated by thin solid line and thick solid line respectively. Others are same as those in Fig. 3.

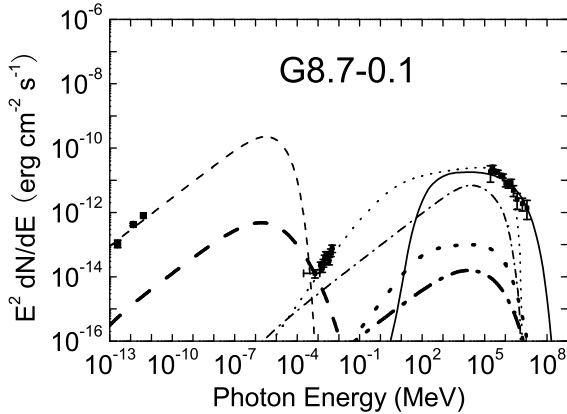


Figure 5. The comparison of detailed spectra calculated by the model with the observations for the SNR G8.7–0.1. The parameters are same as those for panel (c) in Fig. 4. Synchrotron (dashed line), bremsstrahlung (dotted line), Compton (dash-dotted line) of the primary electrons (thin) and the secondary e^{\pm} pairs (thick), meson decay due to the p-p interaction (black solid line) are indicated in the figure.

higher energies are mainly from the p-p interactions due to the high-energy protons collide with the ambient matter.

3.2 SNR G23.3–0.3

HESS J1834–087 is another extended TeV source recently discovered in the *HESS* survey of the inner Galaxy in VHE γ -rays. The source, which is spatially coincident with the SNR G23.3–0.3 (W41), has a size of 12 arc minutes and a γ -ray flux of 8% of the flux from the Crab Nebula above 200 GeV, with a photon index of 2.45 ± 0.16 (Aharonian et al. 2006b). Moreover, Albert et al. (2006) presented the observations of HESS J1834–087 with the Major Atmospheric Gamma Imaging Cherenkov telescope (*MAGIC*), and the differential γ -ray flux can be expressed as $dN/dAdtdE = (3.7 \pm 0.6) \times 10^{-12} (E/\text{TeV})^{-2.5 \pm 0.2} \text{ cm}^{-2} \text{ s}^{-1} \text{ TeV}^{-1}$.

G23.3–0.3 is an asymmetric shell-type SNR with radio and X-ray photons having been detected. In radio band, the SNR has a spectral index of 0.5 and a flux of 70 Jy at 1 GHz (Green 2006). Moreover, Tian et al. (2007) reported new H I observations from the VLA Galactic Plane System and a new *XMM-Newton* observation for HESS J1834–087. They concluded that G23.3–0.3 is an old SNR with a distance of $4 \pm 0.2 \text{ kpc}$ and an age of $\sim 10^5 \text{ yr}$. Furthermore, a density of 6 cm^{-3} was estimated around the SNR from the VGPs H I line emission associated with the SNR (Tian et al. 2007). The new *XMM-Newton* observation indicated diffuse X-ray emission within the *HESS* source and suggested an association between the X-ray and the VHE γ -ray emission. The intrinsic X-ray spectrum from 2 to 10 keV could be characterized as a heavily absorbed power law with a flux of $7.0 \times 10^{-13} \text{ erg s}^{-1} \text{ cm}^{-2}$, and a photon index of $2.0_{-0.8}^{+0.7}$ (see details in Tian et al. 2007).

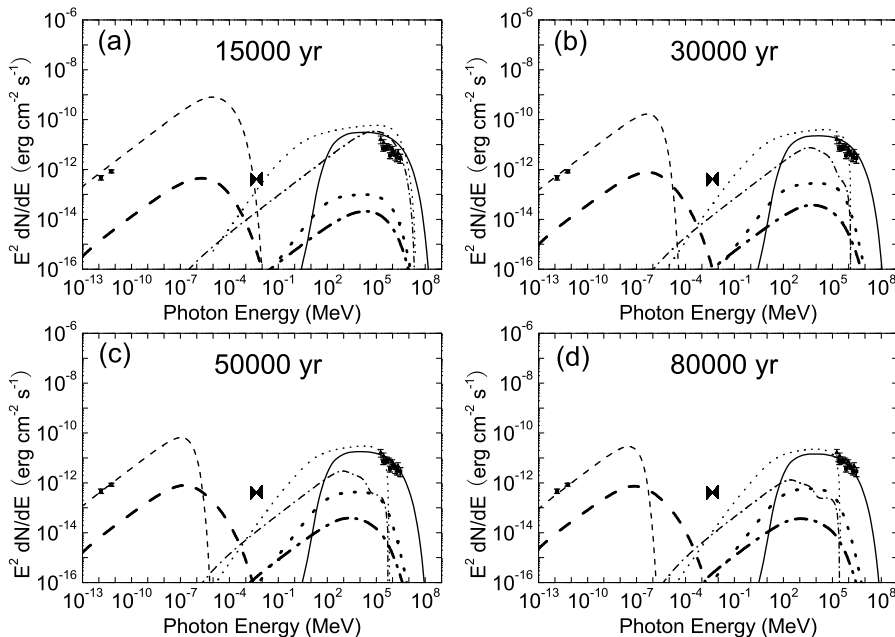


Figure 6. Comparisons of the calculated spectra with the observations for the SNR G23.3–0.3 at different ages. Synchrotron (dashed line), bremsstrahlung (dotted line), Compton (dash-dotted line) of the primary electrons (thin) and the secondary e^\pm pairs (thick), meson decay due to the p-p interaction (black solid line) with radio, X-ray (Tian et al. 2007), and VHE γ -ray with *HESS* (Aharonian et al. 2006b) and *MAGIC* (Albert et al. 2006) observational results are indicated in the figure. The other parameters are $M_{\text{ej}} = 1.5 M_\odot$, $n_{\text{ISM}} = 6 \text{ cm}^{-3}$, $B_{\text{ISM}} = 5 \mu\text{G}$, $K_{\text{ep}} = 0.2$, a distance of 4 kpc, and an age of (a) 15000 yr, (b) 30000 yr, (c) 50000 yr, (d) 80000 yr.

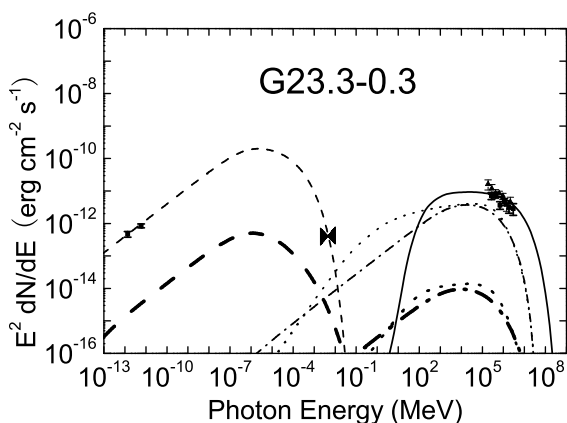


Figure 7. The comparison of detailed spectra calculated by the model with the observations for the SNR G23.3–0.3 with an age of 29800 yr. The other parameters are $M_{\text{ej}} = 1.5 M_\odot$, $n_{\text{ISM}} = 1.5 \text{ cm}^{-3}$, $B_{\text{ISM}} = 8 \mu\text{G}$, $K_{\text{ep}} = 0.05$, and a distance of 4 kpc. Others are same as those in Fig. 6.

We now apply the model in this paper to the old SNR G23.3–0.3, which has been observed in radio, X-ray and VHE γ -ray bands. Firstly, using the similar process as that for the SNR G8.7–0.1, we find K_{ep} must be about 0.2 for the SNR G23.3–0.3 with parameters, a distance of 4 kpc,

$M_{\text{ej}} = 1.5 M_\odot$, $n_{\text{ISM}} = 6 \text{ cm}^{-3}$, $B_{\text{ISM}} = 5 \mu\text{G}$, and an age of several 10^4 yr. Fig. 6 shows the resulting spectra for different ages. For these parameters, the radiative age is 1.43×10^4 yr and then the emission in each panel of Fig. 6 is in the radiative phase. The observations in X-ray band can be explained as the synchrotron and bremsstrahlung radiation of the primary electrons for an age of 15000 yr, however, the calculated results are significantly high above the VHE γ -ray observations by *HESS* and *MAGIC* (see panel (a) in Fig. 6). When the radiative SNR ages, the cut-off energy of the primary electrons decreases quickly and the high-energy protons undergo both catastrophic energy losses due to the p-p collisions and energy-dependent diffusion. As a result, the roll-off energy of the synchrotron radiation of the primary electrons decreases quickly and the number of the TeV photons from the SNR reduces too. We can see from panel (d) in Fig. 6 that the radio and VHE γ -ray observations can be explained by the model with an age of 80000 yr, however, the observed flux in the X-ray band can not be reproduced. To make the model results consistent with the flux of the observations in the X-ray band, the age of the SNR should not be much bigger than the radiative age of the SNR. Furthermore, a smaller n_{ISM} should be chosen to make the calculation spectrum in the VHE γ -ray band consistent with the *HESS* and *MAGIC* observations.

Finally, n_{ISM} is chosen to be 1.5 cm^{-3} with other parameters an age of 2.98×10^4 yr, $M_{\text{ej}} = 1.5 M_\odot$, $B_{\text{ISM}} = 8 \mu\text{G}$, $K_{\text{ep}} = 0.05$ to model the multi-band non-thermal

emission from the SNR G23.3–0.3 and the resulting spectra are shown in Fig. 7. The radiative age for these parameters is 2.97×10^4 yr and the roll-off energy of the synchrotron radiation of the primary electrons is not reduced mostly with an age of 2.98×10^4 yr. It is obvious from Fig. 7 that (1) the emission from the primary electrons dominates that from the secondary e^\pm pairs in all bands and the emission from radio and X-ray band is mainly from the synchrotron radiation of the primary electrons; (2) the TeV photons are produced mainly via the p-p interaction.

4 CONCLUSIONS AND DISCUSSIONS

In this paper, by taking into account the evolution of secondary e^\pm pairs produced via the p-p interaction due to high-energy protons collide with the ambient matter in an SNR, we developed a time-dependant model of multi-waveband non-thermal particle and photon spectra both for young and for old shell-type SNRs. The primary electrons accelerated directly by the shock wave usually dominate the secondary e^\pm pairs produced from the p-p collisions for a young SNR, however, the emission from the secondary e^\pm pairs becomes more and more important and eventually surpasses the radiation from the primary electrons as the SNR grows old because the source of the primary electrons is cut off and the synchrotron radiation loss is significant for electrons when the SNR is in the radiative phase, whereas the secondary e^\pm pairs can be produced for a long time due to the small cross section for the p-p interaction (see Fig. 2). K_{ep} , which can not be directly deduced from the observations now and is usually limited by comparison of the model results with the multi-band observations for a given SNR, is also a crucial parameter to determine whether the contribution to the final non-thermal emission of the secondary e^\pm pairs dominates that of the primary electrons. For an old SNR with small K_{ep} , the non-thermal photons with energies < 10 MeV are usually produced mainly via the radiations of the secondary e^\pm pairs (see Fig. 2).

The model is applied to two old shell-type SNRs, G8.7–0.1 and G23.3–0.3, whose VHE γ -rays are detected in the *HESS* survey of the inner Galaxy. G8.7–0.1 is a shell-type SNR with an age of ~ 15000 yr. The SNR must be in the radiative phase to make the calculated results consistent with the *Chandra* X-ray observations. Finally, a set of parameters, a distance of 6 kpc, an age of 18000 yr, $M_{ej} = 1.5 M_\odot$, $n_{ISM} = 6 \text{ cm}^{-3}$, $K_{ep} = 0.15$, and $B_{ISM} = 6 \mu\text{G}$ is used to model the multi-wavelength non-thermal emission from the SNR G8.7–0.1. It can be concluded that (1) the radio emission from the SNR is mainly from the synchrotron radiation of the primary electrons, whereas the non-thermal photons with energies around 0.1 keV primarily come from the synchrotron radiation of the secondary e^\pm pairs produced from the p-p collisions; (2) the observed X-ray photons with energies ranging from 2 to 10 keV are produced mainly via the bremsstrahlung of the primary electrons; (3) the TeV photons with energies < 1 TeV are primarily from both the bremsstrahlung of the primary electrons and the p-p collisions of the primary protons, however, those with higher energies are produced mainly through the p-p interaction (see Fig. 5). Another old SNR is G23.3–0.3, which is an asymmetric shell-type SNR and spatially coincide with

HESS J1834–087. Tian et al. (2007) reported new H I observations from the VLA Galactic Plane System and a new *XMM-Newton* observation for HESS J1834–087, and argued that G23.3–0.3 is an old SNR with a distance of 4 ± 0.2 kpc and an age of $\sim 10^5$ yr, moreover, a density of 6 cm^{-3} was estimated around the SNR from the VGPs H I line emission associated with the SNR. We find that, using $n_{ISM} = 6 \text{ cm}^{-3}$ and an age of $\sim 10^5$ yr with other appropriate parameters, the model result agrees with the radio and VHE γ -ray observations, but the calculated X-ray flux is significantly lower than the observed one given by *XMM-Newton* (see Fig. 6). A smaller age and a smaller n_{ISM} are needed to make the calculation result consistent with the multi-band observations. Finally, we use parameters a distance of 4 kpc, $M_{ej} = 1.5 M_\odot$, an age of 2.98×10^4 yr, $n_{ISM} = 1.5 \text{ cm}^{-3}$, $B_{ISM} = 8 \mu\text{G}$, and $K_{ep} = 0.05$ to model the multi-band non-thermal emission from the SNR G23.3–0.3. The modeling results can be consistent with both the radio, VHE γ -ray observations and the X-ray flux with these parameters. Moreover, the emission from the secondary e^\pm pairs is negligible and the multi-wavelength photons with those parameters for the SNR mainly come from the radiation of the primary particles, and the TeV photons primarily have hadronic origin (see Fig. 7).

The model in this paper includes the contribution of the secondary e^\pm pairs produced from the p-p collisions to the non-thermal emission from SNRs. The secondary e^\pm pairs can be produced for a long time and experience energy losses and diffusion, and the contribution of the secondary e^\pm pairs to the final non-thermal emission from an SNR can become more and more important and eventually surpasses that of the primary electrons when the SNR ages in the radiative phase. Whether the contribution of the secondary e^\pm pairs to the final non-thermal emission is prominent or not depends heavily on the SNR age, K_{ep} and n_{ISM} . These parameters can be limited by the comparison of the model result with the multi-wavelength observations for a given SNR, however, the shortage of precise observations and uncertainties such as the initial eject mass and the initial velocity of the shock lessen the reliability of the calculated results. On the other hand, for an old SNR with observed TeV emission, if the TeV photons primarily have hadronic origin, the emission from the secondary e^\pm pairs is usually prominent. The morphology of the resulting spectrum for an SNR in the energy range between 10 MeV to 1 TeV directly relates to the primary origin of the VHE photons. Fortunately, the Gamma Ray Large Area Space Telescope (*GLAST*) have a good sensitivity and resolution in the energy range between 30 MeV and 300 GeV, and the observations with *GLAST* will give a direct evidence on whether the TeV photons from an SNR mainly have hadronic origin or leptonic origin. Obviously, *GLAST* will give more limits on the parameters in the modeling process with the model in this paper for an SNR, and then we can get more insights on the acceleration and photon production processes involved in SNRs.

ACKNOWLEDGEMENTS

We are grateful to H. Bartko for providing the *MAGIC* data points and an anonymous referee for his/her very constructive comments. This work is partially supported by a Dis-

tinguished Young Scientists grant from the National Natural Science Foundation of China (NSFC 10425314), NSFC grant 10463002, NSFC grant 10778702, and grant from the Department of Education of Yunnan Province (07J51074). We appreciate the use of the high performance computer facilities at Yunnan University, Kunming, PRC.

REFERENCES

- Aharonian F. et al., 2004, *Nature*, 432, 75
Aharonian F. et al., 2005, *A&A*, 437, L7
Aharonian F. et al., 2006a, *A&A*, 449, 223
Aharonian F. et al., 2006b, *ApJ*, 636, 777
Albert J. et al., 2006, *ApJ*, 643, L53
Bamba A. et al., 2003, *ApJ*, 589, 253
Bamba A. et al., 2005a, *ApJ*, 621, 793
Bamba A., Yamazaki R., Hiraga J. S., 2005b, *ApJ*, 632, 294
Baring M. G. et al., 1999, *ApJ*, 513, 311
Berezhko E. G., 1996, *ARep*, 40, 155
Berezhko, E. G., Ksenofontov, L. T., Völk, H. J., 2006, *A&A*, 452, 217
Blandford R. D., Eichler D., 1987, *Phys. Rep.*, 154, 1
Blondin J. M. et al., 1998, *ApJ*, 500, 342
Cui W., Konopelko A., 2006, *ApJ*, 652, L109
Dermer C. D., 1986, *A&A*, 157, 223
Ellison D. C., Jones, F. C., Reynolds, S. P., 1990, *ApJ*, 360, 702
Enomoto R. et al., 2002, *Nature*, 416, 823
Fatuzzo M., Melia F., Crocker R.M., 2006, preprint (astro-ph/0602330)
Gaisser T. K., 1990, *Cosmic Rays and Particle Physics*. Cambridge Univ. Press, Cambridge
Green D. A., 2006, *A Catalogue of Galactic Supernova Remnants (2006 April version)*. Astrophysics Group, Cavendish Laboratory, Cambridge, United Kingdom
Kassim N. E., Weiler, K. W., 1990, *Nature*, 343, 146
Katagiri H. et al., 2005, *ApJ*, 313, 842
Kamae T. et al., 2005, *ApJ*, 619, L163
Kamae T. et al., 2006, *ApJ*, 647, 692
Koyama K. et al., 1995, *Nature*, 378, 255
Lazendic J. S. et al., 2004, *ApJ*, 602, 271
Odegard N., 1986, *AJ*, 92, 1372
Pannuti T. G. et al., 2003, *ApJ*, 593, 377
Reynolds S. P., 1996, *ApJ*, 459, L13
Sturmer S. J. et al., 1997, *ApJ*, 490, 619
Tian W. W. et al., 2007, *ApJ*, 657, L25
Yamazaki R. et al., 2006, *MNRAS*, 371, 1975
Zhang L., Fang J., 2007, *ApJ*, 666, 247